DIRECT NUMERICAL SIMULATION OF A TRANSITIONAL BUBBLE IN A COMPRESSIBLE BOUNDARY LAYER

José Roberto Moreto, jose.moreto@usp.br
Elmer Mateus Gennaro, elmer@sc.usp.br
Marcello A. Faraco de Medeiros, marcello@sc.usp.br
Universidade de São Paulo

Abstract. At take off or landing the strong lift generated by the lifting surfaces promotes high suction peaks at significant regions of the boundary layer. Compressibility effects are important in these regions despite the low Mach number of the airplane. Although this occurs more often in the slat, it also can occur at the main element or the air-flap. Therefore, the compressible separated flow has a significant influence on aircraft aerodynamics even at low Mach numbers. At these conditions, an important phenomenon that occurs is the transitional bubble and has significant impact on the aerodynamic performance. The study of transitional bubbles requires a numerical approach, since there is no analytical method to describe this phenomenon. One way to perform a numerical simulation of a transitional compressible bubble, improving the numerical performance, is using pre-processed laminar compressible boundary layer which imposes an adverse pressure gradient. Firstly the similarity profile is obtained by the Illingworth-Stewartson similarity transformation. which will be used as an initial condition for Direct Numerical Simulations (DNS). The use of a similar profile in order to stablish the base flow reduce abruptly the computational cost to obtain the base flow, the convergence with a better accuracy can be achieved with less than 100 time steps while without the similar profile was necessary more then 10000 time steps to achieve an acceptable convergence

Keywords: DNS, similar boundary layer profile,hydrodynamic instability,laminar separation bubble

1. INTRODUCTION

The motivation for the study stems, first of all, from the fact that practical applications in aeronautics most often involve compressibility. This is generally recognized as the cruise condition, where the airplane is at very high speed. Nevertheless, at take off or landing the strong lift generated by the lifting surfaces promotes such high suction peaks that significant regions of the boundary layer experience compressibility effects despite the Mach of the airplane being low. This is the case of the slats, but sometimes occurs in the flat or main element too (van Dam, 2002; Rumsey and Ying, 2002). In the boundary layer on these surfaces under these circumstances, for instance, transition often occurs in an adverse pressure gradient region and transition of the Tollmien-Schlichting type is enhanced by adverse pressure gradient.Another ingredient in these developments was the observation of harmonics in the evolution of wavepackets in natural transition made by Gostelow (2004).

Wavepackets in adverse pressure gradient have already been studied (Seifert, 1995; van Hest *et al.*, 1994). These investigations also indicated that subharmonic resonance was at play in these packets. The detailed investigation on the evolution of modulated waves in channel flow set the path to an explanation that could reconcile these observations. It appeared quite simply that the interaction of wavepackets could lead to oblique transition in boundary layers with or without pressure gradient.

A comprehensive investigation of transition in compressible adverse pressure gradient would involve a very large number of parameters, including, at least, Reynolds number, Mach number, pressure gradient, wave amplitude, and distance between interacting packets. A parametric search would be too expensive and time consuming, and, moreover, the amount of data to be processed and interpreted would be ridiculously large.

In order to reduce the computational time some strategies have been studied as stablish better initial conditions to obtain an accurate base flow with less computational time. Since the focus of the present study is the compressive boundary layer was adopted the Illingworth-Stewartson transformation to obtain a similar profile with heat transfer and pressure gradient.

2. METHODOLOGY

2.1 Formulation

In the current study, the governing equations are the compressible Navier-Stokes equations. The continuity equation is

$$\frac{\partial \rho}{\partial t} + \frac{\partial \rho u_j}{\partial x_j} = 0. \tag{1}$$

The momentum equations for the velocity components in the streamwise, normal and spanwise directions can be written as

$$\frac{\partial \rho u_i}{\partial t} + \frac{\partial \rho u_i u_j}{\partial x_j} = -\frac{\partial p}{\partial x_i} + \frac{\partial \tau_{ij}}{\partial x_j} \tag{2}$$

and the energy equation is

$$\frac{\partial E_T}{\partial t} + \frac{\partial u_j (E_T + p)}{\partial x_j} = -\frac{\partial q_j}{\partial x_j} + \frac{\partial u_j \tau_{ij}}{\partial x_j}, \tag{3}$$

where x_i are the Cartesian coordinates (x,y,z), t is the time, u_i are the velocity components (u,v,w), ρ is the density and p is the pressure. The total energy is given by $E_T = \rho \left(e + \frac{u^2 + v^2 + w^2}{2} \right)$ and the primitive variable e is the internal energy. The non-dimensional constitutive relations for a Newtonian fluid and Fourier heat conduction are

$$\tau_{ij} = \frac{1}{Re} \left(\frac{\partial u_i}{\partial x_j} + \frac{\partial u_j}{\partial x_i} - \frac{2}{3} \frac{\partial u_k}{\partial x_k} \delta_{ij} \right) \tag{4}$$

and

$$q_j = -\frac{1}{(\gamma - 1) M_c^2 Pr Re} \frac{\partial T}{\partial x_j}, \tag{5}$$

where the Prandtl number is defined as $Pr = \frac{c_p \, \mu}{k}$, γ is the ratio of specific heat, c_p is the specific heat at constant pressure and k is the thermal conductivity. The Reynolds number of the flow is defined as

$$Re = \frac{\rho_\infty U_\infty \, \delta^*}{\mu_\infty}. \tag{6}$$

The dimensional variables $(\rho_\infty, U_\infty, \mu_\infty)$ are the density, the velocity and the dynamic viscosity of the free stream. The parameter δ^* is the displacement thickness.

The perfect-gas law for non-dimensional pressure and temperature is

$$p = (\gamma - 1) \, \rho \, e \tag{7}$$

and

$$T = \frac{\gamma M^2 p}{\rho}. \tag{8}$$

These conservation equations were presented with the following non-dimensionalization scheme

$$u_i = \frac{u_i^\dagger}{U_\infty}, \qquad \rho = \frac{\rho^\dagger}{\rho_\infty}, \qquad p = \frac{p^\dagger}{\rho_\infty U_\infty^2}, \qquad T = \frac{T^\dagger}{T_\infty},$$

$$t = \frac{t^\dagger U_\infty}{\delta_{\omega_0}^\dagger}, \qquad x_i = \frac{x_i^\dagger}{\delta_{\omega_0}^\dagger}, \qquad \alpha = \alpha^\dagger \delta_{\omega_0}^\dagger, \qquad \omega = \frac{\omega^\dagger \delta_{\omega_0}^\dagger}{U_\infty}, \tag{9}$$

where α is the streamwise wavenumber and ω is the radial frequency. The superscript (†) indicates dimensional parameters. For viscosity the Sutherland model was employed.

2.2 Numerical method

Simulations performed in the current work required high accuracy of the numerical solution (Lele (1992); Souza (2003)). Compact finite-difference schemes were then adopted. The compact schemes for spatial derivatives are extremely attractive when explicit time advancement schemes are used. The most popular compact scheme for spatial derivatives, also called Padé scheme, is the symmetric sixth order version. This scheme is symmetric and does not exhibit dissipative errors. In the current implementation this approximation was used only for the interior points.

For compact schemes, the finite-difference approximations to the derivatives of the function are expressed as a linear combination of the given function values and derivatives on a set of nodes. First an uniformly spaced mesh was considered where the nodes are indexed by i, which varies from 1 to N. In these schemes the value of f_i' is dependent on all the other nodal values. In general, compact schemes are significantly more accurate for short length scales than non-compact

schemes (Kopal (1961); Collatz (1966)). Lele (1992) emphasizes the importance of using methods of high-order and show schemes with 6th order approximation for the interior of the mesh.

Here, the following 6th order compact scheme for the first derivatives was used

$$f'_{i-1} + 3f'_i + f'_{i+1} =$$
$$\frac{1}{12h}(f_{i-2} + 28f_{i-1} - 28f_{i+1} - f_{i+2}) + O(h^6). \tag{10}$$

In the equation above, h is the grid spacing. For the second derivative, successive first derivatives were taken. This is know to be less accurate than a direct calculation of the second derivative. Nevertheless, when viscosity is not constant this requires many more terms to be calculated with severe implications on the computer resources needed. 2nd order approximations were use at and next to most boundaries. Tests were performed with this and other schemes. The results showed that the numerical scheme was more stable with 2nd order approximations than high order schemes. It is emphasized that, for a sufficiently long distance from the shear zone, it is possible to use low order without reducing the overall accuracy of the simulations. At a generic boundary $i = 1$, the scheme for first derivative can be written as

$$f'_1 = \frac{1}{2dy}(-3f_1 + 4f_2 - f_3) + O(h^2). \tag{11}$$

For the points next to the boundary, $i = 2$,

$$f'_2 = \frac{1}{2dy}(-f_1 + f_3) + O(h^2). \tag{12}$$

For the points at the opposite boundary, $i = N$ and $i = N - 1$, similar approximations were used.

At the wall, high accuracy had to be maintained. For that purpose, high order compact asymmetric schemes were derived in line with Souza *et al.* (2005); Silva *et al.* (2009).

The time-advancement of the computational variables (ρ, ρu_i, E_t) was obtained by a 4th order Runge-Kutta method. The scheme used here works in four step (Ferziger and Peric (1997)). The combination of these steps results in 4th order accuracy.

The non-linear terms in the Navier-Stokes equation can produce aliasing errors. In order to remove this error a high-order compact filter was implemented (Lele (1992)). The numerical filter was applied after the last step of the Runge-Kutta scheme. This filter consists in recalculating the distribution of the primitive variables and is of 4th order accuracy. The filter is given by

$$0.1702929\,\widehat{f}_{i-2} + 0.6522474\,\widehat{f}_{i-1} + \widehat{f}_i + 0.6522474\,\widehat{f}_{i+1} +$$
$$0.1702929\,\widehat{f}_{i+2} = \frac{0.001359850}{2}\,f_{i-3} + \frac{0.3333548}{2}\,f_{i-2} +$$
$$\frac{1.3211800}{2}\,f_{i-1} + 0.9891856\,f_i + \frac{1.3211800}{2}\,f_{i+1} +$$
$$\frac{0.3333548}{2}\,f_{i+2} + \frac{0.001359850}{2}\,f_{i+3} + O(h^4). \tag{13}$$

Implementation of the filtering schemes on domains with non-periodic boundaries requires the near boundary nodes to be treated separately. Therefore near the boundaries the following formulas of 4th order accuracy were used

$$\widehat{f}_1 = \frac{15}{16}f_1 + \frac{1}{16}(4f_2 - 6f_3 + 4f_4 - f_5), \tag{14}$$

$$\widehat{f}_2 = \frac{3}{4}f_2 + \frac{1}{16}(f_1 + 6f_3 - 4f_4 + f_5), \tag{15}$$

$$\widehat{f}_3 = \frac{5}{8}f_3 + \frac{1}{16}(-f_1 + 4f_2 + 4f_4 - f_5). \tag{16}$$

They were of the non-compact type.

2.3 Grid stretching

The governing equations can be transformed from a Cartesian coordinate system to any general orthogonal coordinate system. Hence a non-uniformly spaced computational grid in the physical plane can be transformed into uniformly spaced grid in the computational plane.

Simple transformations can be used to cluster grid points in regions of large gradients, where more resolution is required. Here, in the points near the free stream the problem permits less resolution, while close to the wall greater resolution is needed. Therefore, it is possible to stretch the grid and decrease the overall number of points used while maintaining the overall accuracy.

In this work a formula from Anderson (1990) giving a constant stretching was adopted. τ is a stretching parameter that varies from zero (no stretching) to large values. It produce the most refinement near $y = y_c$, which is located at the wall as seen in equations

$$y = y_c \left\{ 1 + \frac{\sinh[\tau(\eta - B)]}{\sinh(\tau B)} \right\} \tag{17}$$

where

$$B = \frac{1}{2\tau} \ln \left[\frac{1 + (e^\tau - 1)(y_c/H)}{1 + (e^{-\tau} - 1)(y_c/H)} \right].$$

In equation (17), the parameter H is the size of the computational domain. In order to apply this transformation to the governing equations, partial derivatives have to be taken. For the first derivatives one has

$$\frac{\partial f}{\partial y} = \frac{\partial f}{\partial \eta} \frac{\partial \eta}{\partial y}, \tag{18}$$

where

$$\frac{\partial \eta}{\partial y} = \frac{\sinh(\tau B)}{\tau y_c \sqrt{1 + [(y/y_c) - 1]^2 \sinh(\tau B)^2}}. \tag{19}$$

This relation should be used in combination with the compact schemes. Applying relation (18) to the derivative approximations, the following tridiagonal compact scheme for the first derivatives is obtained

$$\kappa \psi'_{j-1} \left. \frac{\partial f}{\partial y} \right|_{j-1} + \psi'_j \left. \frac{\partial f}{\partial y} \right|_j + \kappa \psi'_{j+1} \left. \frac{\partial f}{\partial y} \right|_{j+1} =$$
$$a \frac{f_{j+1} - f_{j-1}}{\delta \eta} + b \frac{f_{j+2} - f_{j-2}}{\delta \eta}, \tag{20}$$

where $\psi'_j = \frac{1}{\partial \eta/\partial y}$. The parameters κ, a e b can be defined according to the compact finite-difference scheme used. Grid stretching was also used to provide a buffer zone at the outer flow and the outflow boundary conditions. This was important to prevent wave reflection at the computational boundaries (Lele, 1992). However, for wavepacket that are localized in space, the buffer zone did not have to be long.

2.4 Initial condition

In order to improve the accuracy and reduce the computational time, especially in cases with adverse pressure gradient was used an initial condition based on similarity equations.These equations are obtained using the Illingworth-Stewartson transformation (Cohen and Reshotko, 1955)

The Illingworth-Stewartson similar transformation is defined as follows:

$$\tilde{x} = \int_0^x b \frac{p_1 c_1}{p_0 c_0} dx \tag{21}$$

$$\tilde{y} = \frac{c_1}{c_0} \int_0^y \frac{\rho_1}{\rho_0} dy \tag{22}$$

where subscript 0 refers to the stagnation flow conditions and the subscript 1 refers to conditions in the external flow (at the outer edge of boundary layer) at station x. $\tilde{x}, \tilde{y}$ are the transformed independent variables,b is the Sutherland law of

viscosity coefficient p_1, p_0 are respectively the pressure at the outer flow and stagnation pressure, c_1, c_0 are the sound velocity at outer flow and stagnation sound velocity, and ρ_1, ρ_0 are the flow density at the outer flow and stagnation flow density.

$$\tilde{u}_1 = K\tilde{x}^m \tag{23}$$

Equation 23 define a potential edge flow, where K is an arbitrary constant and m defines the flow angle.

Applying Eq. (21),Eq. (22) and Eq.(23) into the equations for conservation of mass, momentum and energy yields the following compressible boundary-layer system are reduce to ordinary differential equation system.where the prime denotes differentiation with respect to η.

$$\left.\begin{array}{rcl} f''' + ff'' & = & \beta(f'^2 - 1 - S) \\ S'' + PrS' & = & (1 - Pr)\left[\frac{(\gamma-1)M_e^2}{1+\frac{\gamma-1}{2}M_e^2}(f'f''' + f''^2)\right] \end{array}\right\} \tag{24}$$

Where f' is the velocity profile u/U_∞, S is the enthalpy, and M_e is the Mach number. The system (24) is subject to the following boundary conditions:

$$\begin{array}{llll} \eta = 0 & : & \eta = \infty & : \\ & f(0) = 0 & & f'(\infty) = 1 \\ & f'(0) = 0 & & S(\infty) = 0 \\ & \frac{\partial S}{\partial \tilde{y}} = 0 \quad \text{Adiabatic} & & \\ or & S = S_w \quad \text{Isothermal} & & \end{array} \tag{25}$$

3. TESTS

As seen on Eq. (25) some boundary conditions to solve the EDO Eq.(24) is defined at $\eta = \infty$, therefore to solve the equations was necessary the use of a "shooting" method. The boundary conditions $f''(0)$ and $S'(0)$ are estimated and are performed the integration then the value of $f'(\eta_{max})$ and $S(eta_{max})$ are compared with the boundary conditions. Combining the 4th order Runge-Kutta integration and the Newton-Raphson method the $f''(0)$ and $S(0)$ are determined. This results was compared with various profiles calculates by Cohen and Reshotko (1955), the velocity derivative $f''(\eta) = du/d\eta$ and enthalpy derivatives are shown in Tab.1, Tab.2 and Tab. 3

Table 1. Similar boundary layer profile, boundary conditions (cooled wall $S_w = -1.0$)

	Cohen and Reshotko (1955)		Present Work	
β	$f''(\eta)$	$S'(\eta)$	$f''(\eta)$	$S'(\eta)$
-0.360	0.2448	0.4001	0.2447463	0.3998986
-0.14	0.4166	0.4544	0.4170893	0.4560052
0.00	0.4696	0.4696	0.4696000	0.4696000
0.50	0.5806	0.5806	0.5811425	0.4942201
2.00	0.7381	0.5203	0.7386403	0.5206301

Table 2. Similar boundary layer profile, boundary conditions ($S_w = 0.0$)

	Cohen and Reshotko (1955)		Present Work	
β	$f''(\eta)$	$S'(\eta)$	$f''(\eta)$	$S'(\eta)$
2.00	1.6870	0.0000	1.6872182	0.0000000
1.60	1.5213	0.0000	1.5215140	0.0000000
1.00	1.2326	0.0000	1.2325877	0.0000000
0.00	0.4696	0.0000	0.4696000	0.0000000
-0.16	0.1905	0.0000	0.1907798	0.0000000

Some similar profiles are shown:

Table 3. Similar boundary layer profile, boundary conditions (heated wall $S_w = 1.0$)

β	Cohen and Reshotko (1955)		Present Work	
	$f''(\eta)$	$S'(\eta)$	$f''(\eta)$	$S'(\eta)$
-0.10	0.1805	-0.4033	0.1813599	-0.4032299
0	0.4696	-0.4696	0.4696000	-0.4696000
0.50	1.2351	-0.5725	1.2348059	-0.5728858
1.00	1.7368	-0.6154	1.7366841	-0.6155853
2.00	2.4878	-0.6613	2.4876846	-0.6614548
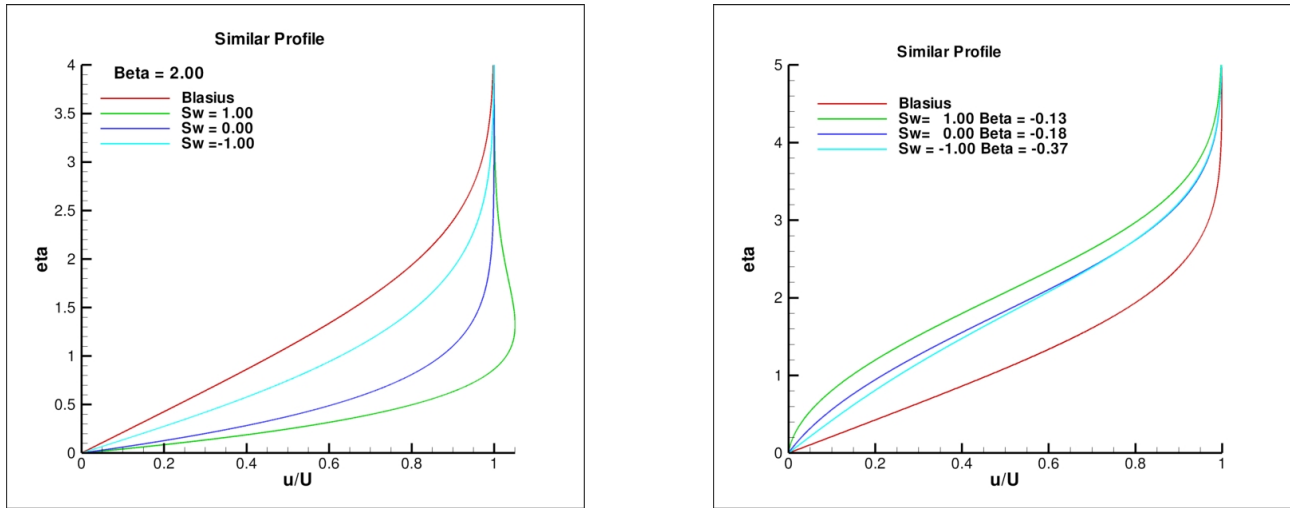
Figure 1. The similar u velocity profile, for various wall temperatures on the left and the near the separation on the right

4. RESULTS

To evaluate the initial conditions effect on the base flow accuracy and convergence rate was simulated some cases with the similar profile as initial condition and without this profile as initial condition.

In order to verify the convergence was defined the relative error:

$$u_{err} = \frac{|u_{err(t)} - u_{err(t-1)}|}{|u_{err(t)}| + 1} \tag{26}$$

$$v_{err} = \frac{|v_{err(t)} - v_{err(t-1)}|}{|v_{err(t)}| + 1} \tag{27}$$

The unit summation on the denominator is necessary to avoid errors when the velocity is null.

The following figures show the calculated u velocity error for the domain central point.

Is remarkable the increase of the convergence rate when the use of similar profile as initial condition. We can see Fig.(2) that the convergence of the base flow with the initial profile presents an error less than $5.0 \cdot 10^{-4}$ before 50 time step, on the other hand the base flow establishment without the similar profile as initial condition present divergence around 800 time steps. Note that the base flow without an similar profile as initial condition presents an error above $5.0 \cdot 10^{-4}$ even after 2000 time steps Fig.(3). Moreover from Fig.(4) and Fig.(5) we note the base flow velocities, without
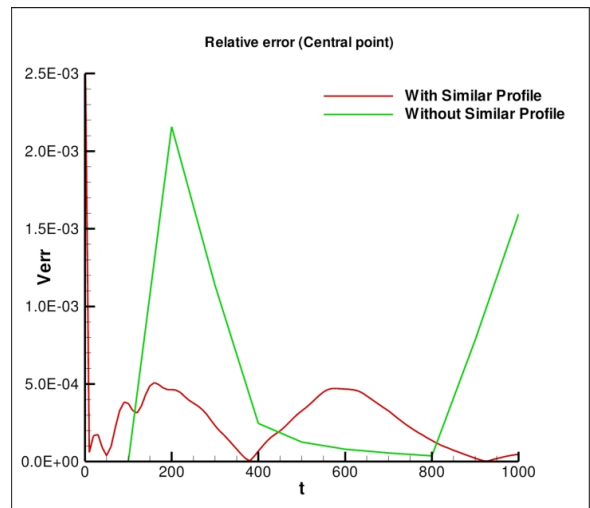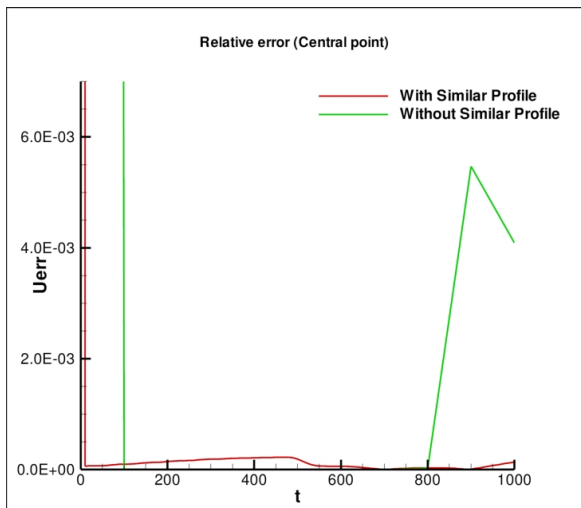
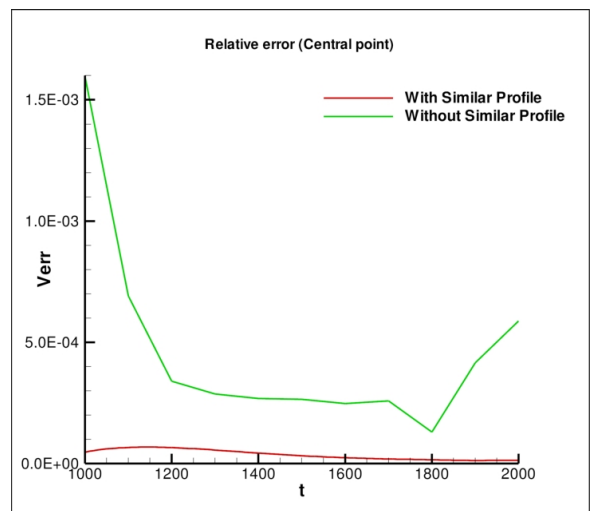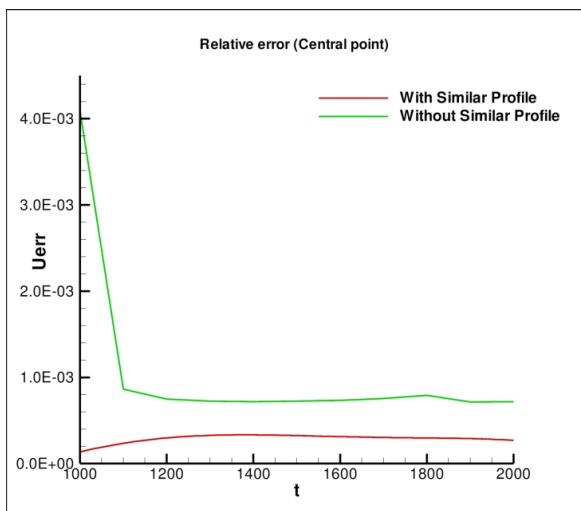Figure 2. u,v velocities relative errors 1000 time steps

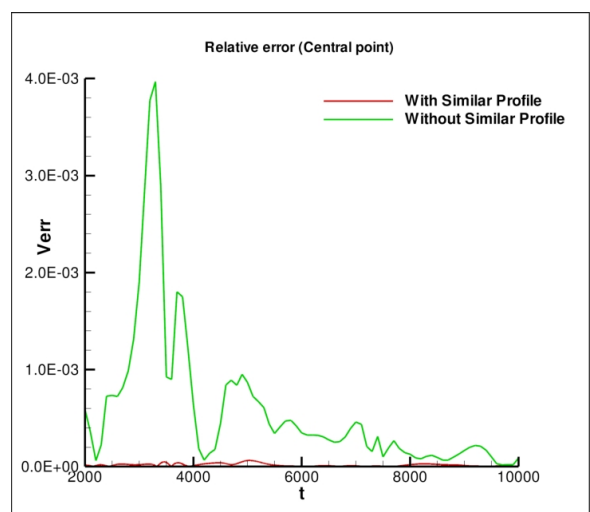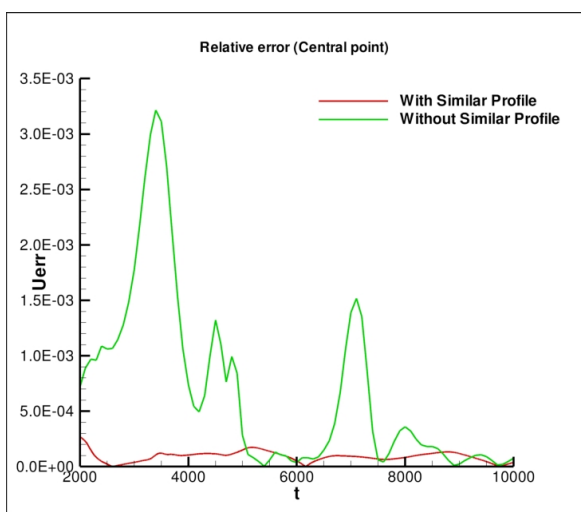Figure 3. u,v velocities relative errors 2000 time steps

Figure 4. u,v velocities relative errors 10000 time steps

the similar profile, oscillates reaching an error at $1.0 \cdot 10^{-3}$ and the base flow velocities errors, with the similar profile, was established under $5.0 \cdot 10^{-5}$.
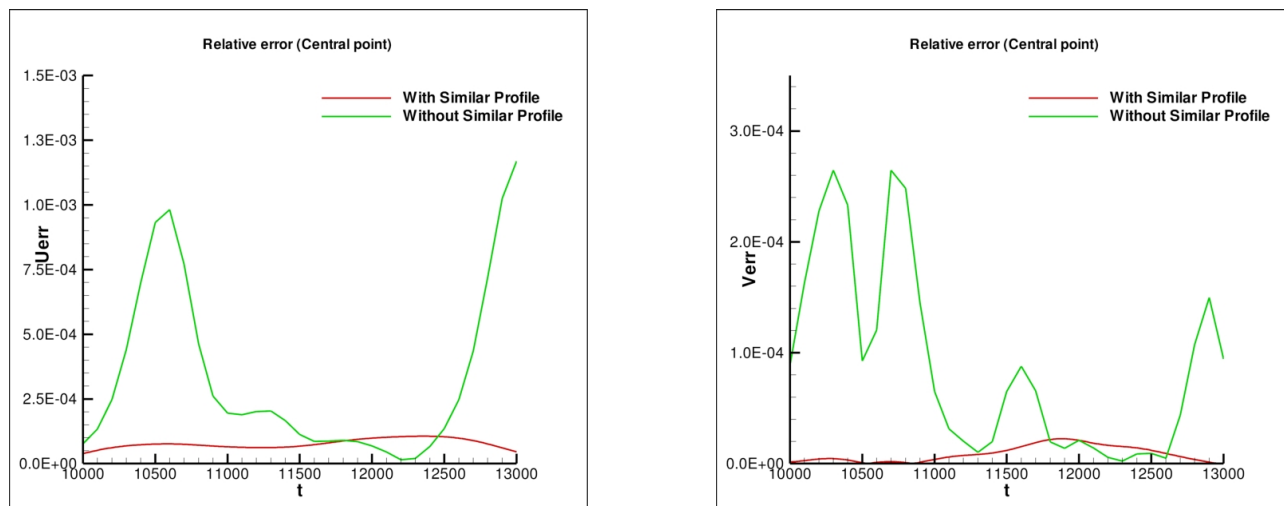
Figure 5. u,v velocities relative errors 13000 time steps

5. FINAL REMARKS

The results showed that using a similar profile to generate the base flow a better accuracy is achieved and the computational cost can be abruptly reduced. As a comprehensive investigation of transition in compressible adverse pressure gradient would involve a very large number of parameters, including, at least, Reynolds number, Mach number, pressure gradient, wave amplitude is necessary a speed up on the code convergence. This can be achieved by stablish the base flow by similar transformations, as showed on section 4. In that way complete parametric studies, about the laminar bubble separation phenomenon, and the discussion of the results from the physical perspective will be presented at the time of the conference.

6. ACKNOWLEDGEMENTS

7. REFERENCES

Anderson, J.D., 1990. *Modern Compressible Flow*. McGraw-Hill.

Cohen, C.B. and Reshotko, E., 1955. "Similar solutions for the compressible laminar boundary layer with heat transfer and pressure gradient".

Collatz, L., 1966. *The numerial treatment of differential equations*. Springer–Verlag.

Ferziger, J.H. and Peric, M., 1997. *Computational methods for fluid dynamics*. Springer-Verlag.

Gostelow, J.P., 2004. "Effect of strong adverse pressure gradients and incident wakes on transition and calming". In R. Govindarajan and R. Narasimha, eds., *IUTAM Symposium on Laminar-turbulent transition*. Springer-Verlag, Bangalore - India, pp. 133–138.

Kopal, Z., 1961. *Numerial analysis*. Chapman & Hall, 2nd edition.

Lele, S.K., 1992. "Compact finite difference schemes with spectral-like resolution". *J. Comp. Phys.*, Vol. 103, pp. 16–42.

Rumsey, C.L. and Ying, S.X., 2002. "Prediction of high hift: review of present CFD capabilities". *Prog. Aero. Sciences*, Vol. 38, pp. 145–180.

Seifert, A., 1995. "Non-linear evolution of point-source disturbances in an adverse pressure gradient laminar boundary layer". In *IUTAM Conference on nonlinear instability and transition in tri-dimensional boundary layers*. Manchester.

Silva, H.G., Souza, L.F. and Medeiros, M.A.F., 2009. "Verification of a mixed high-order accurate dns code for laminar-turbulent transition by the method of manufactured solutions". *Int. J. Num. Meth. Fluids.* Accepted.

Souza, L.F., Mendonça, M.T. and Medeiros, M.A.F., 2005. "The advantages of using high order finite difference schemes in laminar-turbulent transition studies". *Int. J. Numer. Meth. Fluids.* , Vol. 48, pp. 567–582.

Souza, L.F., 2003. *Instabilidade Centrífuga e transição para turbulência em escoamentos laminares sobre superfícies côncavas*. Ph.D. thesis, ITA - Brasil.

van Dam, C.P., 2002. "The aerodynamics design of multi element high-lift systems for transport airplanes". *Progress in Aerospace Sciences*, Vol. 38, pp. 101–144.

van Hest, B.F.A., Passchier, D.M. and van Ingen, J.L., 1994. "The development of a turbulent spot in an adverse pressure

gradient boundary layer". In R. Kobayashi, ed., *Laminar–turbulent transition*. IUTAM, Springer-Verlag, Sendai—Japan.